Detection of tar brown carbon with the single particle soot photometer (SP2)

Joel C. Corbin [1] and Martin Gysel-Beer [2]

[1]Metrology Research Centre, 1200 Montreal Road, National Research Council Canada, Ottawa, ON K1A 0R6, Canada
[2]Laboratory of Atmospheric Chemistry, Paul Scherrer Institute, 5232 Villigen PSI, Switzerland

Correspondence: Joel Corbin (Joel.Corbin@nrc-cnrc.gc.ca)

Abstract.

We investigate the possibility that the refractory, infrared-light-absorbing carbon particulate material known as "tar balls" or tar brown carbon (tar brC) generates a unique signal in the scattering and incandescent detectors of the single particle soot photometer (SP2). As recent studies have defined tar brC in different ways, we begin by reviewing the literature and proposing a material-based definition of tar. We then show that tar brC results in unique SP2 signals due to a combination of complete or partial evaporation, with no or very little incandescence. Approximately 70% of tar particles incandesced. At the time of incandescence the ratio of light scattering to incandescence from these particles was up to twofold greater than from soot black carbon (BC). In our sample, where the mass of tar was threefold greater than the mass of soot, this led to a bias of < 5% in SP2-measured soot mass, which is negligible relative to calibration uncertainties. The enhanced light scattering of tar is interpreted as due to its being more amorphous and less graphitic than soot BC. The fraction of the tar particle which does incandesce was likely formed by thermal annealing during laser heating.

These results indicate that laser-induced incandescence, as implemented in the SP2, is the only BC measurement technique which can quantify soot BC concentrations separately from tar, while also potentially providing real-time evidence for the presence of tar. In contrast, BC measurement techniques based on thermal–optical ("EC") and absorption ("eBC") measurements cannot provide such distinctions. The optical properties of our tar particles indicate a material similarity to the tar particles previously reported in the literature. However, more- and less-graphitized tar samples have also been reported, which may show stronger and weaker SP2 responses, respectively.

1 Introduction

Atmospheric light-absorbing carbon (LAC) in particulate matter (PM) plays a substantial role in the radiative balance of the earth both directly and by influencing cloud properties (Boucher et al., 2013). While soot black carbon (soot BC) is the best-recognized form of LAC (Bond et al., 2013), increasing attention has recently been paid to the so-called "brown carbon" (Kirchstetter et al., 2004; Laskin et al., 2015) and "tar balls" (Pósfai et al., 2004; Hand et al., 2005; Niemi et al., 2006; Semeniuk et al., 2006; Tivanski et al., 2007; Alexander et al., 2008; Vernooij et al., 2009; Chakrabarty et al., 2010; Adachi and Buseck, 2011; China et al., 2013; Zhu et al., 2013; Tóth et al., 2014; Hoffer et al., 2016a, b; Sedlacek III et al., 2018; Corbin et al., 2019)

25 which possess substantially different physical properties than BC. The term "brown carbon" is canonically used to refer to the collection of substantially light-absorbing organic molecules found in PM, while the term "tar balls" refers to the insoluble amorphous-carbon spheres which may be produced by the pyrolysis of high-molecular-weight fuels such as biomass (Tóth et al., 2014) or heavy fuel oil (Corbin et al., 2019). Here we will refer to these two sub-types of brown carbon as "soluble brown carbon" (soluble brC) and "tar brC" following Corbin et al. (2019). Both forms of brC may comprise a large fraction of the light

30 absorption of atmospherically-relevant aerosols such as wildfire smoke (Lack et al., 2012; China et al., 2013; Liu et al., 2015) and marine-engine exhaust (Corbin et al., 2018b, 2019).

The distinction between soluble brC, tar, and soot BC is important as it may result in unique environmental fates and impacts of these distinct types of LAC, due to their unique chemical and morphological properties (Corbin et al., 2019). Similarly, "BC" instruments designed to measure soot BC based on one of its defining properties – insolubility in water and organic

35 solvents; refractoriness up to ~ 4000 K; a structure consisting primarily of sp^2-bonded graphene-like carbon; and a morphology of aggregated monomers of diameter 10–80 nm (Bond et al., 2013; Petzold et al., 2013) – may be cross-sensitive to soluble brC or tar. Cross-sensitivities to soluble brC are generally limited to the BC instruments measuring light absorption at shorter visible wavelengths of 300–500 nm, which normally report their measurements as equivalent BC (eBC, Petzold et al. 2013). Cross-sensitivities to tar brC are more problematic, and include both eBC measured at visible and near-infrared wavelengths of

40 300-1000 nm, as well as and thermal–optically defined elemental carbon (EC) (Corbin et al., 2019).

The fact that tar brC may absorb substantially at wavelengths of 1000 nm implies a further potential cross-sensitivity of instruments such as the single-particle soot photometer (SP2), which relies upon a continuous-wave 1064 nm Nd:YAG laser to heat particles to incandescence. The SP2 is normally used to report single-particle rBC mass concentrations by calibrating incandescence signals with reference to BC particles of known mass and composition. Therefore, any cross-sensitivities of SP2

45 rBC to tar brC would require that tar be refractory enough to reach the >3000 K attained by soot BC.

However, an SP2 cross sensitivity to tar brC may also occur indirectly, if a tar brC sample is capable of undergoing complete or partial annealing to rBC during heating by the SP2 laser. This would result in an incandescence signal from rBC which did not exist prior to the measurement. A recent study by Sedlacek et al. (2018) suggested that this effect may lead to apparent rBC signals of up to 9% of the total particle mass, for laboratory-generated tar brC. Their tar brC measurements could not distinguish

50 whether this signal was due to the formation of rBC during tar-brC formation versus in-SP2 annealing. Sedlacek et al. (2018) also performed experiments using nigrosin (a polyaniline-based dye) to demonstrate that laser-induced annealing may contribute 45% of the incandescence signal expected for pre-existing rBC. This percentage decreased with increasing laser power, to 25%, demonstrating that evaporation may occur more rapidly than annealing under appropriate conditions (including high laser power density and low degree of graphitization in the starting material). It is interesting to note that Moteki and Kondo (2008)

55 also measured nigrosin in an SP2 but observed zero laser-induced annealing. This may reflect variability in the experimental procedures or in the composition of the nigrosin.

Corbin et al. (2019) reported that the apparent rBC mass of tar particles (that is, the magnitude of any cross-sensitivities) produced by a marine engine operated on heavy fuel oil was negligible. Their inference was based on the fact that thermal–optical EC (IMPROVE-A protocol) remained high while rBC signals fell to zero, under conditions where the aerosol AAE (the negative

60 slope of a log-log plot of absorption against wavelength) was ~ 2, corresponding to low engine loads. They also found a negligible response of the Soot-Particle Aerosol Mass Spectrometer (SP-AMS; Onasch et al. 2011), which also relies on the absorption of a 1064 nm laser, to these tar particles. Note that any comparison of the SP2 and SP-AMS sensitivities should be made with caution, as particles experience lower pressure, shorter beam exposure times, and different laser-power densities in the latter instrument (laser power densities are unmeasured and may vary between instruments). The lack of SP2 cross-sensitivity to

65 tar brC in Corbin et al. (2019) is likely related to the fact that tar brC is less refractory than soot BC, and therefore not capable of reaching incandescent temperatures prior to vapourization. Another potential factor, that the mass-specific absorption efficiency (MAE or "MAC") of the tar brC was 23-fold smaller than that of soot BC at 950 nm wavelength, (although it was only 5-fold smaller at 660 nm and 2-fold smaller at 370 nm). The MAE is fundamentally related to refractoriness, because both MAE and refractoriness will increase with increasing degree of graphitization of the tar (Corbin et al., 2019), as will be discussed further

70 later.

A negligible incandescence signal in the SP2 does not mean that the SP2 is incapable of detecting tar brC, because the SP2 does not only measure time-resolved incandescence signals but also time-resolved scattering signals. Previous work has exploited the time-resolved SP2 scattering signals, particularly relative to the time of incandescence, to determine apparent rBC coating thicknesses (Gao et al., 2007; Laborde et al., 2012a) and to differentiate core-shell rBC particles from "attached" rBC

75 particles (BC particles coagulated with, but not engulfed by, non-BC particles, Moteki et al. 2014).

From this basis, the present manuscript explores the possibility that a detailed analysis of the time-resolved signals allows the detection of tar brC particles by SP2 in terms of their (predicted) anomalous scattering signals. We also seek to quantify the potential interference of tar on SP2 incandescence. We use data from Corbin et al. (2019) for our analysis, contrasting a tar-containing sample with a tar-free sample from the same engine. The manuscript is structured as follows. In Section 2 we

80 review previous work on the properties and definition of tar brC. In Section 3, we give a technical discussion of the SP2, present the test data set used below, and describe the analysis techniques used in this study. In Section 4, we present the results of this study.

2   Definition and properties of tar brC

2.1   Review of properties

85 The particles referred to as "tar balls" or "tar brC" in the literature generally have consistent properties. Physically, tar brC exists as spheres of solid, amorphous-carbon-like material, and may exist as isolated spheres (Pósfai et al., 2004) or as aggregates thereof (Girotto et al., 2018). The isolated or aggregated tar particles are of diameters 100–300 nm, approximately one order of magnitude larger than the corresponding monomer diameter in soot aggregates, 10–80 nm (Corbin et al., 2019). Unlike the soluble organic molecules (soluble brC) typically addressed by brC studies (Laskin et al., 2015; Moschos et al., 2018), tar brC is

90 insoluble and vapourizes at about 1000 K (Corbin et al., 2019).

Tar brC consists primarily of carbon but contains impurities of hydrogen and oxygen (Tóth et al., 2018). Tar brC emitted from biomass burning may contain impurities of K, Cl, Si, and S (Pósfai et al., 2004). Atmospheric tar brC have also been

reported which contained impurities of S and Si, but not K (Alexander et al., 2008; Zhu et al., 2013), which has been proposed as indicating an origin of heavy-fuel-oil combustion (Corbin et al., 2019).

95   In terms of their optical properties, tar particles may be considered a subset of brC, as their imaginary refractive index decreases with increasing wavelength (Alexander et al., 2008; Corbin et al., 2019), which results in a brown appearance at appropriate concentrations (Liu et al., 2016). However, light absorption by tar remains significant even in in the near-infrared (880 nm) (Alexander et al., 2008; Corbin et al., 2019). This light absorption has been described by the Tauc band-gap model, which predicts a slow tailing off of absorption with increasing wavelength (Corbin et al., 2019).

100   In terms of its molecular structure, tar is best considered as a subclass of the solid carbon materials which lie along a continuum of graphitization rather than a complex mixture of discrete molecules (like soluble brC) (Corbin et al., 2019). The carbon in tar is much less graphitized than the carbon in soot BC; that is, tar has a higher sp^3/sp^2 bonding ratio than BC (Tóth et al., 2018; Corbin et al., 2019).

Here we emphasize that a "continuum of graphitization" does not mean that brC and BC are formed by a simple one-
105   dimensional process of graphitization, and does not mean that tar brC is incompletely-formed soot BC. Studies such as Saleh et al. (2018) should not be misinterpreted as suggesting this. First, kinetic limitations to the graphitization process mean that movement along the "continuum" may be limited for a given starting material (Corbin et al., 2019). Second, there is some evidence for tar formation during atmospheric processing (Pósfai et al., 2004; Sedlacek III et al., 2018), and not only during thermal annealing (Tóth et al., 2014; Corbin et al., 2019). Third, the small diameters of soot-BC monomers fundamentally
110   influence the molecular structure (Parent et al., 2016) and (consequently as well as independently) the optical properties of soot-BC aggregates (Liu and Mishchenko, 2005). The fundamental differences in molecular structure and morphology of tar compared with soot-BC reflect fundamentally different formation pathways; the two LAC types are not simply points along a one-dimensional continuum (Corbin et al., 2019).

The formation of tar brC has been proposed to proceed through the pyrolysis of high-molecular-weight fuels including biomass
115   (Tóth et al., 2014) and heavy fuel oil (Corbin et al., 2019), or by the atmospheric processing of primary biomass-burning particles (Pósfai et al., 2004; Sedlacek III et al., 2018). Whereas the pyrolysis hypothesis has been directly demonstrated by laboratory studies for both biomass tar (Tóth et al., 2014) and heavy fuel oil tar (Jiang et al., 2019), the atmospheric-processing hypothesis is based on less direct evidence from two aircraft-based studies. In the first study, Pósfai et al. (2004) used electron microscopy to observe tar ball number fractions increasing from a negligible amount to 85% in a smouldering fire over Mozambique after
120   about 1h of atmospheric processing. It must also be mentioned that Pósfai et al. (2004) also observed a tar ball number fraction of 18% for a separate unprocessed plume over South Africa. In the second study, Sedlacek III et al. (2018) also concluded that tar ball number and mass fractions increasing with plume age. They quantified tar ball number fractions by electron microscopy, and tar ball mass fractions under the assumption that their tar balls flash-vapourized at 873 K in an aerosol mass spectrometer (which may not be true for processed tar balls, and which was not observed for other samples (Corbin et al., 2019)). The
125   chemical mechanism by which photochemical aging may produce amorphous-carbon spheres material is unclear, and should be investigated in future work.

2.2 Definition

As stated above, the term "tar balls" refers to the insoluble amorphous-carbon spheres which may be produced from the pyrolysis of high-molecular-weight fuels such as biomass (Tóth et al., 2014) or heavy fuel oil (Corbin et al., 2019), and also by atmospheric

130 processing (Sedlacek III et al., 2018). In this manuscript, we have not measured particle morphology, so we use the term "tar brC" to refer to this material, following Corbin et al. (2019). Other literature definitions are as follows.

The term "tar balls" was introduced by Pósfai et al. (2004) to describe the spherical, amorphous-carbon particles found in biomass burning smoke which were stable under the electron beam of a transmission electron microscope. This definition is inconvenient for studies which have not used electron microscopy, which cannot assert stability under an electron beam and may

135 not be able to assert sphericity. In addition, later work by Girotto et al. (2018) showed that "tar ball aggregates" may also exist. We therefore prefer the chemically-based definition given above.

Recently, Sedlacek III et al. (2018) described tar balls as processed primary particles, based on their observations of tar balls appearing to form during atmospheric processing. These observations are corroborated by those of Pósfai et al. (2004), who also measured more tar balls in more-processed wildfire plumes. However, we propose that this definition would be more useful and

140 less ambiguous if inverted. Rather than restricting the term tar balls to processed primary particles (a definition which relies on knowledge of particle history), we allow that atmospheric processing may form tar balls. We then define tar based on its material properties as given above.

This inclusive, material-based definition avoids the unnecessary confusion of requiring a separate name for the tar-like particles measured in unprocessed wildfire plumes (Pósfai et al., 2004; Semeniuk et al., 2006; Adachi and Buseck, 2011; China

145 et al., 2013); in laboratory biomass smoke (Vernooij et al., 2009; Chakrabarty et al., 2010); in fresh marine-engine exhaust (Corbin et al., 2019; Jiang et al., 2019); or in atmospheric air masses of unmeasured or unreported photochemical age (Niemi et al., 2006; Hand et al., 2005; Tivanski et al., 2007; Alexander et al., 2008; Zhu et al., 2013). As all of these particles possess similar material properties, a single name is most appropriate for them. Minor differences such as the formation of oxygenated interfaces due to atmospheric processing (Tivanski et al., 2007) are best considered as forming subcategories within the category

150 of tar.

3 Methods

3.1 Technical description of the Single Particle Soot Photometer (SP2)

The single particle soot photometer (SP2; Droplet Measurement Technologies, CO, USA) is designed to quantify the mass of BC in single particles by laser-induced incandescence (LII, Stephens et al., 2003; Schwarz et al., 2006). Particles exiting a nozzle at

155 near-atmospheric pressure are guided by a sheath flow through into a continuous-wave, intracavity, 1064 nm Nd:YAG laser over the course of roughly 20 μs. If particles are heated to incandescent temperatures by this laser, the resulting incandescent light $I(t)$ is measured by broadband (350–880 nm) and narrowband (350–550 nm) detectors; the broadband signals are normally used due to their greater sensitivity. Elastic scattering of the laser radiation $S(t)$ is measured by a second detector. A third detector

also measures light scattering, but using a four-element avalanche photodiode with the polarity of two elements reversed, such

160   that the measured signal crosses through zero when a particle reaches a specific physical location relative to the detector. This
so-called "split detector" allows the absolute location of a particle in the laser beam to be unambiguously identified, by using the
scattering signals of non-evaporating particles as a measurement of the beam profile (Gao et al., 2007; Laborde et al., 2012a). In
the SP2 used during this study, data were acquired from all detectors every $0.4\,\mu$s. All data in this study were analyzed using the
PSI SP2 Toolkit, version 4.114, to which the novel features discussed below were added.

165   The SP2 scattering detector was calibrated by reference to polystyrene latex sphere standards of diameter 269 nm. The
incandescence detectors of the SP2 were calibrated using mass-selected rBC particles with mass-specific incandescence
responses similar to diesel-engine rBC (Alfa Aeser Inc., FS, Lot #FS12S011). As LII signals are influenced by the material
properties of the rBC (Laborde et al., 2012b; Michelsen et al., 2015), it should be kept in mind that the mass calibration for
different materials (such as the rBC in soot or tar) may be different.

170   The SP2 detects rBC cores with mass (or volume-equivalent size, considering a void-free material density of $1800\,\mathrm{kg\,m^3}$)
from $\sim 0.7\,\mathrm{fg}$ ($\sim 80\,\mathrm{nm}$) to $\sim 200\,\mathrm{fg}$ ($\sim 600\,\mathrm{nm}$). Smaller rBC particles can also be detected, although with reduced counting
efficiency (Laborde et al., 2012c). For canonical soot BC, the integrated mass obtained by SP2 has been validated as accurate
by multiple independent studies over more than a decade (Slowik et al., 2007; Kondo et al., 2011; Laborde et al., 2012c). A
substantial amount of work has also employed the SP2 to investigate the internal mixing or "coating" of rBC with volatile

175   materials (Liu et al., 2017, and references therein). Further details of the SP2 analysis of the present data sets are presented in
Corbin et al. (2018b).

At least two conditions must be met for particles to incandesce in the SP2. First, they must experience a substantial net
heat input from the 1064 nm laser (over a period of $20\,\mu$s, due to the particle velocity through the laser). This corresponds
to a minimum required MAE, so that the heating rate exceeds conductive, evaporative, and other cooling rates (Michelsen

180   et al., 2015; Bambha and Michelsen, 2015). In the SP2, the major cooling mechanism is conductive heat transfer (Bambha and
Michelsen, 2015), which has been reported as limiting its ability to detect spark-generated carbon nanoparticles (Gysel et al.,
2012). The heating rate will depend most strongly on the material properties of the particle; these properties may themselves be
influenced by the heating process if annealing occurs (Michelsen et al., 2015; Sedlacek et al., 2018). Second, particles must be
refractory up to $\sim 3000\,\mathrm{K}$, so that the corresponding incandescence is detectable (Schwarz et al., 2006). Particles types which

185   meet these conditions include canonical soot BC (Schwarz et al., 2006) and metal-containing particles such as dust (Moteki
et al., 2017) and volcanic ash (M. Gysel, unpublished data). Particle types which do not meet these conditions include canonical
non-absorbing materials and tar brC. Non-absorbing materials (such as volatile organics, sulfates, and nitrates) will not absorb
the SP2 heating laser and are not refractory. Tar brC may absorb the SP2 heating laser, but is generally only refractory to about
$1000\,\mathrm{K}$ (Corbin et al., 2019). Other forms of brC neither absorb substantially above $\sim 500\,\mathrm{nm}$ (Kirchstetter et al., 2004; Laskin

190   et al., 2015; Moschos et al., 2018) nor are refractory (Lack et al., 2012).

3.2 Test data set

The test data set used here is a subset of the experiments described in previous publications (Corbin et al., 2018b, a, 2019) and summarized in the introduction. The subset of the data set used here corresponds to a single marine engine operated on the same heavy fuel oil (HFO) at the same engine load, but with the engine tuning parameters varied such that either a pure-BC or a tar-rich aerosol resulted (Corbin et al., 2019). We define the relative importance of BC or tar in the samples according to the Absorption Ångström Exponent (AAE) calculated from the wavelength pair $370, 950\,\mathrm{nm}$. This AAE(370,950) was close to 1.0 for the pure-BC case and ~ 2.0 for the tar-rich case. The tar-rich case did *not* correspond to a pure-tar aerosol, but rather one in which the rBC/EC mass ratio was 0.18, and in which over half of the total light absorption at $950\,\mathrm{nm}$ was due to tar and not soot BC. The pure-BC case corresponded to an rBC/EC ratio of 0.97.

In the analysis herein, the pure-BC case is used as a control case while the tar-rich case is used to identify features unique to tar particles. The two cases were measured on the same day using the same sampling configuration.

3.3 Analysis methods

Our analysis methodology employs two fundamental quantities, the calculation of which are described in this section and summarized in Table 1.

3.3.1 Time-resolved scattering cross-section $C(t)$

To quantify tar evaporation in the absence of incandescence, we calculated the time-resolved partial scattering cross-section $C(t)$ of all particles in the test data sets. This procedure has been described in detail by Laborde et al. (2012b) and is illustrated in Figure 1. Briefly, the SP2 split detector is used to define the absolute position of particles in the SP2 laser. The effective laser beam shape is then determined as the median of all measured non-incandescing particles above a user-selected noise threshold. (We inspected the data to ensure that most non-incandescing particles were also non-evaporating.) Calibrated scattering signals are then normalized to this idealized beam shape to obtain $C(t)$.

Above the noise threshold, $C(t)$ is a constant for non-evaporating particles. For evaporating particles, $C(t)$ decreases due to the decreasing particle volume and, potentially, changing refractive index of the particle (Moteki and Kondo, 2008; Laborde et al., 2012b). We therefore used the change in $C(t)$ as a method to identify evaporation and quantify the number fraction of evaporating particles. We calculate the ratio of $C(t)$ at two selected times relative to the mode intensity of the laser beam, defined by $R(t_1, t_2)$ with the times given in terms of laser beam intensity:

$$R(-20\%, 20\%) = \frac{C(-20\%)}{C(20\%)} \tag{1}$$

where $C(-20\%)$ represents $C(t)$ at the time when an incoming particle reaches 20% of the laser-beam maximum for the first time. Conversely, $C(+20\%)$ represents $C(t)$ at the time when a particle reaches 20% of the laser-beam maximum for the second time and has almost left the laser beam.

We note that the PSI SP2 Toolkit has long used $C(t)$ for so-called "leading-edge only" (LEO) analysis (Gao et al., 2007). The calculation of $C(t)$ described above and by Laborde et al. (2012b) is equivalent to a LEO fit of an empirical beam shape function (rather than a prescribed function such as a Gaussian, and without the constraint of fitting to the leading edge). The results presented below are therefore an extension of a previously validated and published approach. We also note that our method for to detecting evaporating tar particles bears some similarity to the method of Moteki et al. (2014) for detecting attached BC particles.

3.3.2 Scattering cross-section at incandescence, $C(t_o)$

To investigate $C(t)$ after the evaporation of volatile material, we define $C(t)$ at the time of incandescence as $C(t_o)$. As was also the case in earlier versions of the PSI SP2 Toolkit, $C(t_o)$ was defined as the scattering signal which occurred just prior to the onset of incandescence. The condition "just prior to" is necessary because the filter used in front of the SP2 scattering detector transmits a portion of the incandescence signal, and because rBC particles may swell during heating (Bambha and Michelsen, 2015). The t_o was defined as $2.4\,\mu s$ seconds before t_i, the time of maximum incandescence signal. This is illustrated in Figure 1.

We note that earlier versions of the PSI SP2 Toolkit also retrieved $C(t_o)$ and used it to constrain the apparent refractive index of rBC, $m_{\mathrm{rBC}} = (n, k)$. Because the precise value of m_{rBC} is not well constrained and may vary between BC materials, a range of possible values for m_{rBC} have been reported in the literature (Bond and Bergstrom, 2006). These values have been empirically observed to follow the approximate relationship $k \approx (n-1)$, as introduced by Bond and Bergstrom (2006) and discussed further by Moteki et. al. (2010). This empirical relationship is sufficient to constrain m_{rBC} to a single value, within the scope of the Mie approximation used herein. This method was used in Corbin et al. (2018b) to determine a best-fit m_{rBC} of (1.9, 0.8) for this data set, which is similar to the value used by Laborde et al. (2012c) for propane-flame soot but smaller than the value of (2.26, 1.26) often used in SP2 data analysis (Moteki et al., 2010; Taylor et al., 2015).

3.4 Data filtering

The particle-detection events analyzed herein were filtered to remove events with fitted peak heights below a limit of detection (LOD) established by inspecting the smoothness of the measured mass distributions. A higher LOD was applied to events analyzed for $C(t)$. This higher LOD was defined at $C(-3\%)$, which is a standard reference condition for LEO analysis in the PSI SP2 Toolkit and reflects the earliest time at which the signal-to-noise ratio of $C(t)$ becomes acceptable. The LOD at $C(-3\%)$ was determined by inspecting a scatterplot of non-incandescing particle sizes retrieved at $C(-3\%)$ with sizes retrieved at $C(100\%)$, the standard position.

Additional filters were introduced to remove events triggered by noise, events where peak fitting failed (for example, due to the coincidence of two particles within the laser beam and with one particle touching the edge of the acquisition window), and events where the detectors were saturated. The number fraction of particles removed by these filters was negligible. For $C(t)$ data, only particles with a valid split position could be used, which corresponds to a limit of approximately $160\,\mathrm{nm}$ in optical diameter (assuming $m = (1.5, 0)$).

4 Results

In the following discussion we present results which provided useful evidence for the presence of unique signals from tar
particles in the SP2. Appendix A describes some results which did not provide useful evidence.

4.1 Evaporating, non-incandescing particles

Figure 2 shows frequency distributions for $R(-20\%, 20\%)$ (Equation 1) for particles where no incandescence signal was
observed. The figure shows data only for particles with optical diameter of 220 ± 40 nm (assuming $m = (1.5, 0)$) to remove
noise from smaller particles and to simplify interpretation.

The $R(-20\%, 20\%)$ represents the fraction by which the scattering cross-section $C(t)$ of a particle decreased when exiting
the beam (sampled at 20% of the maximum laser fluence) compared to entering the beam (also sampled at 20%). Its value is
close to 1 for a non-absorbing particle and $\ll 1$ for an evaporating particle. Values greater than 1 occur due to random error in
$C(t)$.

For both the soot (control) and tar cases, the vast majority of signals can be described by a gaussian fit as falling within the
range $0.7 < R(-20\%, 20\%) < 1.3$. For the tar case the fitted mean and standard deviation were 1.001 ± 0.001 and 0.279 ± 0.002
respectively. This standard deviation reflects a 27.9% precision in the retrieval of $R(-20\%, 20\%)$. For the tar case, a substantial
but small fraction of the particles in Figure 2 (578 of 14766 or 3.9%) showed $R(-20\%, 20\%) < 0.5$, indicating substantial
evaporation. The $C(t)$ profiles of all of these particles are shown in Figure 3. Note that the majority of particles in this sample
were non-absorbing lubrication-oil particles in the sample, which cannot be quantified separately from non-evaporating tar.
Therefore, the actual number fraction of tar particles which evaporate (relative to tar particles which do not evaporate nor
incandesce) is likely to be significantly higher than the 3.9% given above.

By random inspection of the evaporating particles with $R(-20\%, 20\%) < 0.5$, we selected a representative example and
plotted its time-resolved scattering signals in Figure 1d. The scattering cross-section $C(t)$ of this example particle begins at
a plateau (indicating unchanging particle size and composition) before decreasing to a second plateau (indicating a second
stable configuration), then ultimately evaporating completely. Not all evaporating and non-incandescing particles showed this
secondary plateau, many showed only a continuous evaporation, some showed a partial evaporation and remained at a plateau
(Figure 3). It may be speculated that these plateaus reflect the breakup of tar particles into more- and less-absorbing parts,
with the more-absorbing part being completely evaporated and the less-absorbing part passing through the laser unchanged, in
analogy to the particle breakup that is observed for heavily-coated rBC (Sedlacek et al., 2012; Dahlkötter et al., 2014; Moteki
et al., 2014).

This evaporating, non-incandescing behaviour is unlike any we have previously observed in the SP2. Typically, non-
incandescing particles will show a scattering profile similar to that of Figure 1a, corresponding to constant $C(t)$. Recall that
the beam profiles shown in Figure 1 reflects the median of all non-incandescing particles, and therefore may be interpreted as
illustrating the scattering profile of a typical non-incandescing particle.

285   Evaporating but non-incandescing particles may also be observed in the SP2 when sub-detection-limit rBC is internally-mixed with volatile material. This may result in core-shell particles, which were not observed in the tar-rich nor in the control data set. Alternatively, this may result in the "attachment" of soot particles to non-absorbing droplets, rather than core-shell morphologies. However, again, this should have been observed in our control data set but was not. Finally, the presence of sub-detection-limit rBC would have occurred simultaneously with the presence of larger rBC particles, so that some partially-evaporating and

290   incandescing particles should have been seen (as observed for example by Moteki et al. 2014) if this possibility were significant. No particle breakup was observed in our data; no incandescing particles were observed which had a detectable signal remaining at $C(20\%)$. Therefore, this potential cross-sensitivity can be excluded as affecting our analysis.

4.2   Evaporating and incandescing particles

We investigated the possibility that certain tar particles may incandesce in the SP2 due to laser-induced annealing. This possibility

295   requires distinguishing incandescing tar from incandescing soot BC particles (and potentially internally-mixed tar–soot particles). This distinction could be made using a comparison of the scattering and incandescence signals for tar particles, via the ratio $C(t_o)/I_{\text{peak}}$, under the hypotheses that tar particles either (i) contain a substantial volume of refractory, non-incandescent material at the time of incandescence t_i or (ii) possess a substantially different refractive index at t_i. Our data do not rule out the possibility that both hypotheses are true. These symbols were defined in Table 1. For this calculation, it is important to use

300    $C(t)$ and not $S(t)$, because thickly-coated rBC particles penetrate deeper into the SP2 laser. This results in a higher $S(t)$ for the same $C(t)$, since deeper penetration into the laser corresponds to a greater photon flux incident on the particle. We note that the incandescing material in laser-annealed tar would have a significantly different morphology and possibly also molecular structure than soot BC, which would affect its incandescent properties (Moteki and Kondo, 2010). .

Figure 4 shows $C(t_o)/I_{\text{peak}}$ for the tar and soot (control) cases, plotted as a joint-probability histogram of initial optical

305   diameter. The initial optical diameters correspond to the diameter retrieved from $C(-3\%)$ assuming $m = (1.5, 0)$ and serves to indicate the approximate particle size prior to any evaporation. For soot BC, when the ratio $C(t_o)/I_{\text{peak}}$ is appropriately calibrated, it represents the ratio of optical diameter at t_i to rBC-equivalent diameter at t_i. The ratio would then represent the slope of a plot of the rBC optical diameter (just prior to incandescence) against rBC mass-equivalent diameter (obtained from the incandescence signal), and in this scenario the ratio is constrained as equal to unity during BC-coating-thickness analyses

310   when the appropriate calibrations are applied (Corbin et al., 2018b). For clarity we have therefore applied these calibrations to the data presented in Figure 4, although they do not apply to tar.

Figure 4a shows the $C(t_o)/I_{\text{peak}}$ versus diameter histogram for the soot case. An approximately constant $C(t_o)/I_{\text{peak}}$ is observed as a function of initial optical diameter, as highlighted by the dashed ellipse. Above 200 nm, $C(t_o)/I_{\text{peak}}$ begins to decrease, reaching a value of 0.9, which at least partially reflects the limitations of the Mie model used to calculate the

315   optical diameter in our analysis. The region within this dashed ellipse reflects the SP2 response to soot BC. Inspection of the individual particles within the soot BC region showed the canonical SP2 response, as depicted for a representative particle in Figure 1b. This response involves a scattering signal $S(t)$ that decreases almost simultaneously with incandescence and a scattering cross-section $C(t)$ that drops rapidly after the onset of incandescence.

Figure 4b shows the $C(t_o)/I_{\text{peak}}$ versus diameter histogram for the tar case. Here, in addition to the soot BC region, a second
"cloud" of particles appears at higher $C(t_o)/I_{\text{peak}}$ and higher initial diameter, as highlighted by the solid circle on the figure. The
circle is reproduced on Figure 4a to allow a direct comparison of the two data sets. Inspection of the individual particles within
this "tar region" showed an anomalous SP2 response, as depicted for a representative particle in Figure 1e. Unlike the coated
soot particle, no plateau in $C(t)$ is observed at incandescence, rather, incandescence occurs simultaneously with a continuously
decreasing $C(t)$. After incandescence, $C(t)$ is zero. This behaviour indicates that a substantial amount of refractory material
was internally mixed with the material which incandesced. The material which incandesced may have undergone chemical
transformation during laser heating (laser-induced annealing as discussed above, Sedlacek et al. 2018) or may have been present
prior to laser heating; we consider annealing more likely due to the homogeneous appearance of these tar particles in the electron
microscope (as discussed in Corbin et al., 2019).

The area of Figure 4 containing incandescing tar particles is significantly greater than the area containing soot-BC particles
(that is, the illustrative circle is larger). This indicates that tar particles showed a more variable ratio of non-incandescing to
incandescing material, and/or that the incandescing material varied in degree of graphitization or annealing. This is the expected
behaviour, considering that the annealing process involves the localized crystallization of graphitic domains following thermal
decomposition, or heating-related internal tensions (Franklin, 1951). Such a phase transition would occur at variable times
during laser heating, leading to a variable ratio between evaporated and annealed material, leading to a variable $C(t_o)/I_{\text{peak}}$
ratio.

The clear relationship between $C(t_o)/I_{\text{peak}}$ and initial optical diameter seen in Figure 4b rules out the hypothesis that this
region reflects extremely-thickly-coated soot. Extremely-thick coatings would show no correlation in Figure 4, and would in
some cases display particle breakup, which results in in a non-zero $S(t)$ and $C(t)$ after evaporation (Moteki and Kondo, 2007;
Sedlacek et al., 2012; Dahlkötter et al., 2014). This was never observed in our data set.

Finally, we also present a coated soot-BC particle in Figure 1c in order to illustrate the behaviour of such particles in the
SP2. We emphasize that, unlike all other examples, this particle type was very rare in our data set, and is not representative
of our data set, in which most BC was uncoated (Corbin et al., 2018b). This coated particle shows a $C(t)$ that decreases to
a plateau prior to the onset of incandescence. This is the typical behaviour of coated rBC. The initial decrease indicates the
evaporation of a volatile coating, and the plateau indicates continued heating of the now-uncoated rBC up until the onset of
incandescence at $\sim 3500\,\text{K}$. The onset of incandescence corresponds to a slight increase in $C(t)$, which must be interpreted
in the context of heat-induced swelling and interference of the incandescence signal at the scattering detector (Bambha and
Michelsen, 2015). Overall, the scattering and incandescence profile of this coated soot BC particle is clearly distinct from the
profiles of tar. We note that some particles with extremely-thick rBC coatings or coagulated rBC-droplet morphologies may not
display the above-mentioned plateau due to breakup during evaporation (Sedlacek et al., 2012; Moteki et al., 2014), but such
particles also display a $C(t)$ significantly greater than zero after evaporation, and, as mentioned above, were not observed in our
data set.

5 Discussion

The results presented above show that marine-engine tar particles absorb the 1064 nm SP2 laser with sufficient efficiency to evaporate. In some cases, incandescence accompanied this evaporation, which was attributed to partial laser-induced annealing. While this incandescence-via-partial-annealing phenomenon was directly demonstrated by Sedlacek III et al. (2018) using nigrosin and laboratory-generated tar particles, in our study there is a possibility of rBC pre-existing as an internal mixture with tar. We consider this possibility extremely unlikely based on the unique formation mechanism of tar compared to soot BC, and the fact that tar particles have universally been observed as internally homogeneous in the literature (Section 2).

A competing hypothesis to the partial annealing hypothesis is that the incandescing tar particles were actually coagulated tar–soot-BC particles. We reject this hypothesis, because of the observed late incandescence (in terms of time spent in the laser beam) of tar particles. Coagulation would not result in late incandescence; at worst, it would lead to earlier incandescence due to reduced conductive cooling.

If tar particles absorb 1064 nm light, then they should be measurable by other techniques which employ 1064 nm lasers, such as the Soot-Particle Aerosol Mass Spectrometer (SP-AMS) (Onasch et al., 2012) and pulsed laser-induced incandescence (pulsed LII) instruments (Michelsen et al., 2015). Corbin et al. (2019) explored the response of the SP-AMS to the same tar particles discussed in the present manuscript and found no substantial difference between the mass spectra of tar-containing and tar-free samples. This lack of difference may be due to the different conditions that particles experience within the SP-AMS (including lower pressure, shorter beam exposure times, and different laser power densities, as mentioned in the introduction), or due to the fact that the SP-AMS used in our study did not obtain the single-particle measurements that allowed the SP2 to differentiate between tar and lubrication-oil-related particles. Future work should explore the response of pulsed LII instruments to tar.

The number fraction of evaporating tar particles observed in our data set was 3.9% at 220 ± 40 nm. This fraction is biased by the fact that the majority of particles in our sample were lubrication-oil related (Corbin et al., 2018b). The number fraction of incandescing tar particles was 1324 of 2.62×10^5, or 5.1%. For a given optical diameter, tar particles generated much smaller incandescence signals than soot particles (Figure 4), so that the actual bias in SP2-determined rBC mass concentrations due to tar incandescence was $\ll 5.1\%$. Considering that the mass of tar brC was threefold greater than the mass of soot BC in our measurements (Corbin et al., 2019), this bias is negligible relative to the typical 15% accuracy of an SP2 mass calibration (Laborde et al., 2012c; Taylor et al., 2015).

It cannot be overemphasized that the material referred to as tar or "tar balls" is partially-graphitized, amorphous carbon. There is no therefore no well-defined molecular structure for tar, and a given tar sample may lie at some point along a continuum of graphitization (Bond, 2001; Corbin et al., 2019). While the same is also true of soot BC (Minutolo et al., 1996; Vander Wal et al., 2014), the literature indicates that the range in degree of graphitization of BC emitted by common combustion sources (Bond and Bergstrom, 2006; Zangmeister et al., 2018) is narrower than the corresponding range for tar (Corbin et al., 2019).

Care must therefore be taken when extrapolating the present results to other studies. Certain tar samples may be less graphitic (and less likely to undergo laser-induced evaporation) or more graphitic (and more likely to undergo laser-induced incandescence) than our samples. Based on the wavelength-dependence of absorption of tar in our samples reported and placed in the context of

literature by Corbin et al. (2019) (AAE of about 3), we believe that our tar samples were of a typical degree of graphitization. Future studies should explore the possibility of modulating the SP2 laser power (Sedlacek et al., 2012, 2015), to provide additional information by which tar and soot BC may be distinguished.

6 Conclusions

390   We investigated the response of the SP2 to near-infrared-absorbing, refractory (to about $1000\,\mathrm{K}$) carbonaceous particles ("tar") using a data set in which the presence of tar has been demonstrated, and a control data set in which such particles were absent (Corbin et al., 2019).

By inspecting the time-resolved scattering cross-sections $C(t)$, we found that tar particles can be observed as evaporating but non-incandescing particles in the SP2. Some tar particles also incandesced, either due to laser annealing or possibly due to
395   chemical heterogeneity of the material being referred to as tar. These incandescent tar particles were clearly distinguishable from soot BC according to the ratio of scattering-at-incandescence to incandescence signals. This ratio was a factor of 1.2 to 2.0 greater for tar than for soot BC and much more variable. This high degree of variability would be expected if the incandescent material in these particles formed via the localized crystallization of graphitic domains during laser-induced annealing, such that the molecular composition of the incandescing tar particles may vary significantly.

400   In our data set, we identified 578 and 1324 particles as non-incandescing or incandescing tar particles, respectively. Assuming that the probability of false-negatives is similar for these two cases (in other words, assuming that our different methodologies were not more sensitive to either incandescing or non-incandescing tar), this indicates that about 70% of tar particles produced incandescence signals in the SP2. Future work should employ laboratory-generated tar balls or morphology-based classification to more accurately estimate what fraction of tar particles can be expected to evaporate in the SP2 laser.

405   The analysis presented here shows that an SP2 equipped with a split detector is capable of detecting tar. This makes the SP2, to our knowledge, the only high-throughput technique which has the potential capability of distinguishing tar from soot particles or soluble brC. It remains undetermined whether or not the SP2 signals are useful for the quantification of tar mass or number fractions. Based on the fact that our tar particles had optical properties similar to those reported in other studies (discussed in Corbin et al., 2019), we estimate that our tar particles are of a typical degree of graphitization, such that other tar-containing
410   samples should display similar behaviour to that observed herein. Future work should also explore the possibility of modulating the SP2 laser fluence in order to exploit differences in the absorption efficiencies of tar and soot, while keeping in mind that the material referred to as tar lies on a continuum between amorphous carbon and highly graphitic carbon, such that certain samples will absorb $1064\,\mathrm{nm}$ light more effectively than others, while also most likely being more refractory (Corbin et al., 2019). The techniques used herein may be useful for the future identification of the presence or absence of tar in a sample of unknown
415   composition.

Author contributions

JCC and MGB conceptualized the study; JCC performed the research and drafted the manuscript with input from MGB; MGB developed the original SP2 analysis code which JCC further developed; and MGB acquired funding.

Acknowledgements. This work was supported by the ERC grant ERC-CoG-615922-BLACARAT and by Natural Resources Canada under
420   the Program of Energy Research and Development (PERD). We thank our previous coauthors (Corbin et al., 2018a, 2018b, 2019) for their
contributions to generating the data sets used here.

Table 1. Table of symbols used in the text.

Symbol	Meaning
t	Time spent by a particle in the SP2 laser beam
$S(t)$	SP2 scattering signal
$C(t)$	Scattering cross-section corresponding to $S(t)$
$C(-3\%)$	Scattering cross-section at -3% of laser maximum
	as a particle enters the SP2 laser beam
$I(t)$	SP2 incandescence signal
I_{peak}	SP2 incandescence signal at peak
t_o	Time just before onset of incandescence
t_i	Time of maximum incandescence
$R(-20\%, 20\%)$	Ratio of $C(t)$ at two different t (Eq. 1)

Appendix A: Diagnostics which did not differentiate between tar and the control data set

We attempted to identify evaporating particles using a number of different statistics, with the goal of identifying a parameter which was sensitive to evaporation without requiring the split detector. One motivation for a split-detector-free method is that the new model of the SP2, SP2-XR, does not contain a split detector. Using the region of the scattering signal identified as a peak by the PSI SP2 toolkit, we calculated the full-width-half-maximum (FWHM), the ratio of FWHM to full width, the peak skewness, the mean absolute difference (MAD) between either half of the peak, and the Kolmogorov-Smirnov statistic. These statistics were evaluated by manual inspection and by comparison to $R(-20\%, 20\%)$.

Manual inspection of the MAD suggested that this statistic successfully isolated tar particles, however, in terms of probability density functions, the differences were not different from the control case. Manual inspection of the FWHM of the incandescence peak also suggested a difference for the tar case, but further analysis showed that this difference was due to tar particles penetrating deeper into the laser beam, and therefore experiencing higher heating rates at incandescence. We also explored the use of the Moteki and Kondo (2008) approach to identify evaporating, non-incandescing particles, but did not identify conditions where this method was successful. Based on plots similar to Figure 3 but for various subsets of particles, we believe that alternative approaches must be explored, such as the machine learning approach introduced by Lamb (2019). Alternatively, future work may be able to distinguish tar-containing particles without a split detector if additional instrumental parameters, such as the laser fluence, are varied.
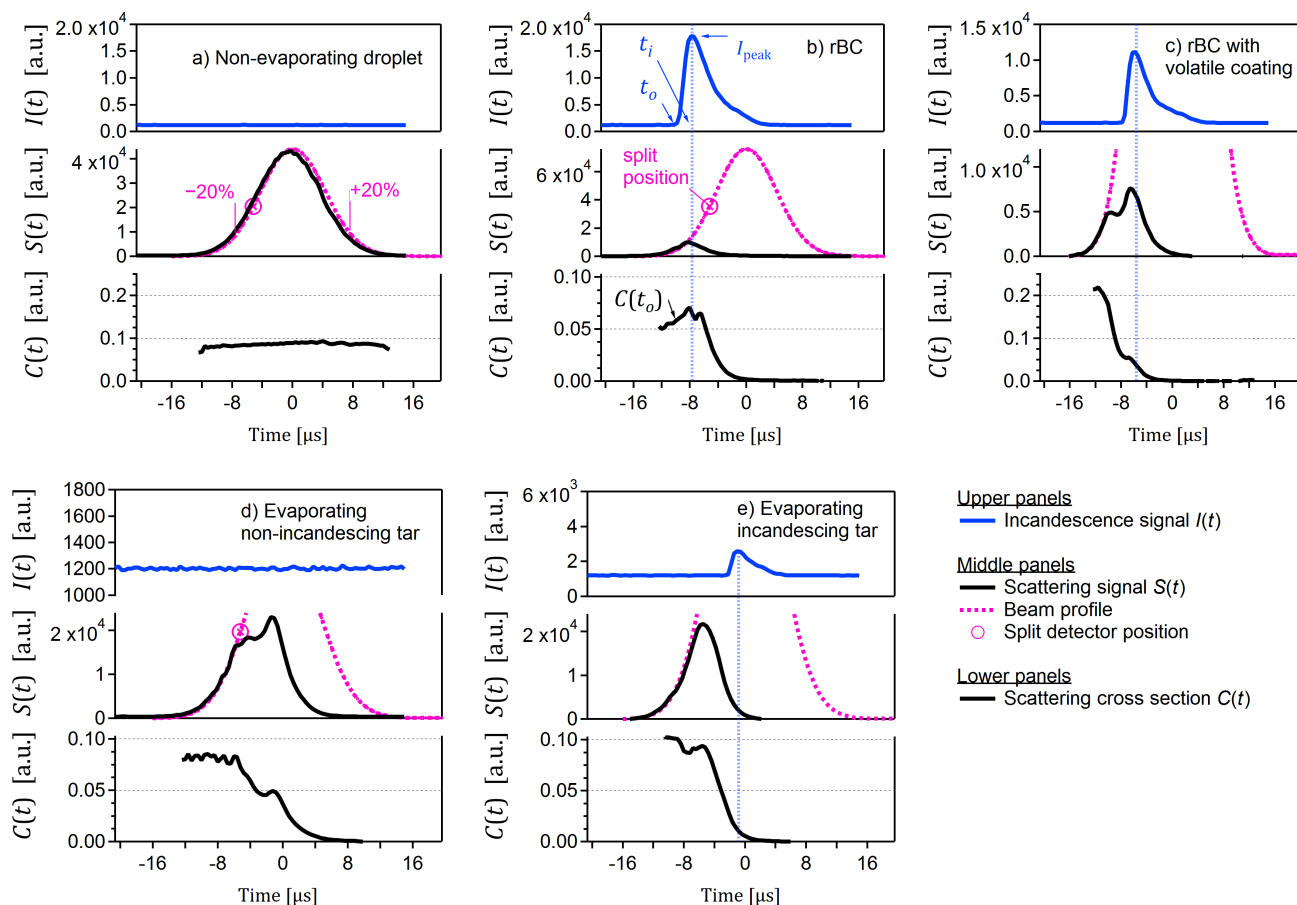
Figure 1. Particle types observed in this study. These examples were selected to be representative of the trends shown in subsequent figures. a) Typical non-absorbing and therefore non-evaporating particle. (Likely lubrication oil / sulfate mixture.) The labels -20% and $+20\%$ indicate fractions of maximum beam intensity. b) Typical soot BC particle. c) Atypical coated soot BC particle (rare in this data set, selected for illustration only). d) Typical evaporating but non-incandescing tar particle. e) Typical evaporating and incandescing tar particle. Note the difference between position of maximum incandescence (vertical blue lines) and position of stable $C(t)$ in panels c) and e), as highlighted by the vertical blue lines. Note also that the ordinate scales vary in order to highlight key features.
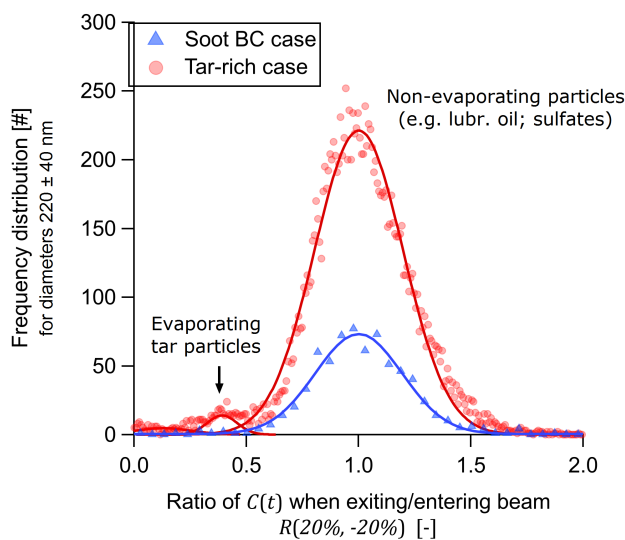
Figure 2. Frequency distribution of the ratio of scattering cross-sections, $R(-20\%, 20\%)$ for non-incandescing particles. curves are Gaussian fits. Ratios were calculated by dividing the second scattering cross-section measurement at 20% of maximum beam fluence (particle exiting the SP2 laser) by the first (particle entering the SP2 laser). Random error in $R(-20\%, 20\%)$ was modelled by gaussian fits, which indicate that about 3.6% of tar-case particles evaporating to less than half of their original cross-section. Note that this 3.6% reflects the fact that the majority of particles in this sample were non-absorbing lubrication-oil particles. In the soot test case, no non-incandescing particles evaporated.
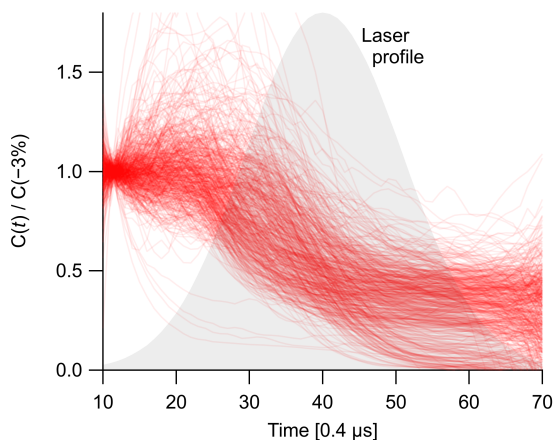
Figure 3. $C(t)$ for all particles with $R(-20\%, 20\%) < 0.5$ in Figure 2, normalized to $C(-3\%)$ (which is normally using for coating-thickness analysis). Each transparent red line represents $C(t)$ for a single particle, as was also shown in the lowest panel of Figure 1d.
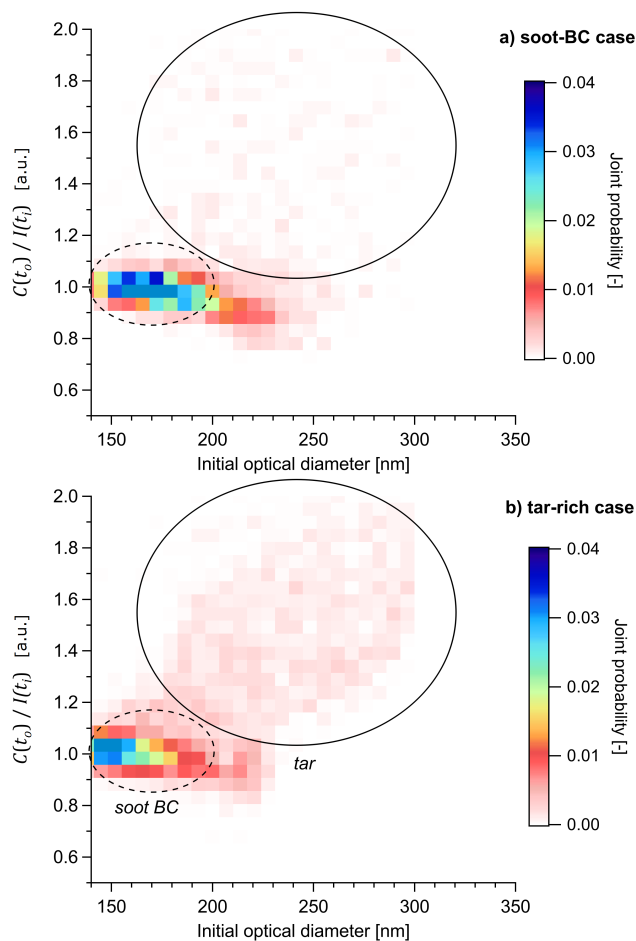
Figure 4. Incandescing tar particles distinguished from soot BC by their scattering properties in the SP2. Scattering cross-section just prior to incandescence ($C(t_i)$; see Figure 1 for illustration) normalized to maximum incandescence signal $I(t_i)$, plotted as a function of particle optical diameter prior to evaporation. Under the condition that the incandescing material is comparable in all cases, an increase in $C(t_i)/I(t_i)$ indicates the presence of non-BC refractory material. Inspection of the data indicated that the joint probability is not exactly equal to zero in the soot-BC case due to coincidence (simultaneous presence of two particles in the laser beam).

References

Adachi, K. and Buseck, P. R.: Atmospheric tar balls from biomass burning in Mexico, J. Geophys. Res., 116, https://doi.org/10.1029/2010jd015102, 2011.

Alexander, D. T. L., Crozier, P. A., and Anderson, J. R.: Brown Carbon Spheres in East Asian Outflow and Their Optical Properties, Science, 321, 833–836, https://doi.org/10.1126/science.1155296, 2008.

Bambha, R. P. and Michelsen, H. A.: Effects of aggregate morphology and size on laser-induced incandescence and scattering from black carbon (mature soot), J. Aerosol Sci., 88, 159–181, https://doi.org/10.1016/j.jaerosci.2015.06.006, 2015.

Bond, T. C.: Spectral dependence of visible light absorption by carbonaceous particles emitted from coal combustion, Geophys. Res. Lett., 28, 4075–4078, https://doi.org/10.1029/2001gl013652, 2001.

Bond, T. C. and Bergstrom, R. W.: Light absorption by carbonaceous particles: An investigative review, Aerosol Sci. Technol., 40, 27–67, https://doi.org/10.1080/02786820500421521, 2006.

Bond, T. C., Doherty, S. J., Fahey, D. W., Forster, P. M., Berntsen, T., DeAngelo, B. J., Flanner, M. G., Ghan, S., Kärcher, B., Koch, D., Kinne, S., Kondo, Y., Quinn, P. K., Sarofim, M. C., Schultz, M. G., Schulz, M., Venkataraman, C., Zhang, H., Zhang, S., Bellouin, N., Guttikunda, S. K., Hopke, P. K., Jacobson, M. Z., Kaiser, J. W., Klimont, Z., Lohmann, U., Schwarz, J. P., Shindell, D., Storelvmo, T., Warren, S. G., and Zender, C. S.: Bounding the role of black carbon in the climate system: A scientific assessment, J. Geophys. Res. Atmos., 118, 5380–5552, https://doi.org/10.1002/jgrd.50171, 2013.

Boucher, O., Randall, D., Artaxo, P., Bretherton, C., Feingold, G., Forster, P., Kerminen, V., Kondo, Y., Liao, H., Lohmann, U., Rasch, P., Satheesh, S., Sherwood, S., Stevens, B., and Zhang, X.: Clouds and Aerosols, Cambridge University Press, http://www.ipcc.ch/report/ar5/wg1/, 2013.

Chakrabarty, R., Moosmüller, H., Chen, L.-W., Lewis, K., Arnott, W., Mazzoleni, C., Dubey, M., Wold, C., Hao, W., and Kreidenweis, S.: Brown carbon in tar balls from smoldering biomass combustion, Atmos. Chem. Phys., 10, 6363–6370, https://doi.org/doi:10.5194/acp-10-6363-2010, 2010.

China, S., Mazzoleni, C., Gorkowski, K., Aiken, A. C., and Dubey, M. K.: Morphology and mixing state of individual freshly emitted wildfire carbonaceous particles, Nat. Comm., 4, n/a–n/a, https://doi.org/10.1038/ncomms3122, 2013.

Corbin, J. C., Mensah, A. A., Pieber, S. M., Orasche, J., Michalke, B., Zanatta, M., Czech, H., Massabò, D., Buatier de Mongeot, C., Mennucci, C., El Haddad, I., Kumar, N. K., Stengel, B., Huang, Y., Zimmermann, R., Prévôt, A. S. H., and Gysel, M.: Trace metals in soot and $PM_{2.5}$ from heavy-fuel-oil combustion in a marine engine, Environ. Sci. Technol., https://doi.org/10.1021/acs.est.8b01764, 2018a.

Corbin, J. C., Pieber, S. M., Czech, H., Zanatta, M., Jakobi, G., Massabò, D., Orasche, J., El Haddad, I., Mensah, A. A., Stengel, B., Drinovec, L., Močnik, G., Zimmermann, R., Prévôt, A. S. H., and Gysel, M.: Brown and black carbon emitted by a marine engine operated on heavy fuel oil and distillate fuels: optical properties, size distributions, emission factors, Journal of Geophysical Research: Atmospheres, 123, 6175–6195, https://doi.org/10.1029/2017JD027818, 2018b.

Corbin, J. C., Czech, H., Massabo, D., Buatier de Mongeot, F., Jakobi, G., Liu, F., Lobo, P., Mennucci, C., Mensah, A. A., Orasche, J., Pieber, S. M., Prévôt, A. S. H., Stengel, B., Tay, L. L., Zanatta, M., Zimmermann, R., El Haddad, I., and Gysel-Beer, M.: Refractory, infrared-absorbing carbon in ship exhaust from heavy fuel oil combustion, npj Atmospheric and Climate Science, https://doi.org/10.1038/s41612-019-0069-5, 2019.

Dahlkötter, F., Gysel, M., Sauer, D., Minikin, A., Baumann, R., Seifert, P., Ansmann, A., Fromm, M., Voigt, C., and Weinzierl, B.: The Pagami Creek smoke plume after long-range transport to the upper troposphere over Europe–aerosol properties and black carbon mixing state,
475   Atmos. Chem. Phys., 14, 6111–6137, https://doi.org/10.5194/acp-14-6111-2014, 2014.

Franklin, R. E.: Crystallite Growth in Graphitizing and Non-Graphitizing Carbons, Proc Royal Soc A: Mathematical, Physical and Engineering Sciences, 209, 196–218, https://doi.org/10.1098/rspa.1951.0197, 1951.

Gao, R. S., Schwarz, J. P., Kelly, K. K., Fahey, D. W., Watts, L. A., Thompson, T. L., Spackman, J. R., Slowik, J. G., Cross, E. S., Han, J.-H., Davidovits, P., Onasch, T. B., and Worsnop, D. R.: A Novel Method for Estimating Light-Scattering Properties of Soot Aerosols Using a
480   Modified Single-Particle Soot Photometer, Aerosol Sci. Technol., 41, 125–135, https://doi.org/10.1080/02786820601118398, 2007.

Girotto, G., China, S., Bhandari, J., Gorkowski, K., Scarnato, B. V., Capek, T., Marinoni, A., Veghte, D. P., Kulkarni, G., Aiken, A. C., Dubey, M., and Mazzoleni, C.: Fractal-like Tar Ball Aggregates from Wildfire Smoke, Environmental Science & Technology Letters, 5, 360–365, https://doi.org/10.1021/acs.estlett.8b00229, 2018.

Gysel, M., Laborde, M., Mensah, A. A., Corbin, J. C., Keller, A., Kim, J., Petzold, A., and Sierau, B.: Technical Note: The single particle soot
485   photometer fails to reliably detect PALAS soot nanoparticles, Atmos. Meas. Tech., 5, https://doi.org/10.5194/amt-5-3099-2012, 2012.

Hand, J. L., Malm, W. C., Laskin, A., Day, D., Lee, T., Wang, C., Carrico, C., Carrillo, J., Cowin, J. P., Collett, J., and Iedema, M. J.: Optical, physical, and chemical properties of tar balls observed during the Yosemite Aerosol Characterization Study, J. Geophys. Res., 110, https://doi.org/10.1029/2004jd005728, 2005.

Hoffer, A., Tóth, A., Nyirő-Kósa, I., Pósfai, M., and Gelencsér, A.: Light absorption properties of laboratory-generated tar ball particles,
490   Atmos. Chem. Phys., 16, 239–246, https://doi.org/10.5194/acp-16-239-2016, 2016a.

Hoffer, A., Tóth, A., Pósfai, M., Chung, C. E., and Gelencsér, A.: Brown carbon absorption in the red and near infrared spectral region, Atmos. Chem. Phys. Discuss., pp. 1–16, https://doi.org/10.5194/acp-2016-452, http://dx.doi.org/10.5194/acp-2016-452, 2016b.

Jiang, L., Elbaz, A. M., Guida, P., Al-Noman, S. M., AlGhamdi, I. A., Saxena, S., and Roberts, W. L.: Cenosphere Formation during Single-Droplet Combustion of Heavy Fuel Oil, Energy & Fuels, 33, 1570–1581, https://doi.org/10.1021/acs.energyfuels.8b03632, 2019.

495 Kirchstetter, T. W., Novakov, T., and Hobbs, P. V.: Evidence that the spectral dependence of light absorption by aerosols is affected by organic carbon, J. Geophys. Res.-Atmos., 109, https://doi.org/10.1029/2004JD004999, 2004.

Kondo, Y., Sahu, L., Moteki, N., Khan, F., Takegawa, N., Liu, X., Koike, M., and Miyakawa, T.: Consistency and Traceability of Black Carbon Measurements Made by Laser-Induced Incandescence, Thermal-Optical Transmittance, and Filter-Based Photo-Absorption Techniques, Aerosol Sci. Technol., 45, 295–312, https://doi.org/10.1080/02786826.2010.533215, 2011.

500 Laborde, M., Crippa, M., Tritscher, T., Jurányi, Z., DeCarlo, P., Temime-Roussel, B., Marchand, N., Eckhardt, S., Stohl, A., and Baltensperger, U.: Black carbon physical properties and mixing state in the European megacity Paris, Atmos. Chem. Phys., 12, 25 121–25 180, https://doi.org/10.5194/acp-13-5831-2013, 2012a.

Laborde, M., Mertes, P., Zieger, P., Dommen, J., Baltensperger, U., and Gysel, M.: Sensitivity of the Single Particle Soot Photometer to different black carbon types, Atmos. Meas. Tech., 5, 1031–1043, https://doi.org/10.5194/amt-5-1031-2012, 2012b.

505 Laborde, M., Schnaiter, M., Linke, C., Saathoff, H., Naumann, K., Möhler, O., Berlenz, S., Wagner, U., Taylor, J., Liu, D., Flynn, M., Allan, J., Coe, H., Heimerl, K., Dahlkötter, F., Weinzierl, B., Wollny, A. G., Zanatta, M., Cozic, J., Laj, P., Hitzenberger, R., Schwarz, J. P., and Gysel, M.: Single Particle Soot Photometer intercomparison at the AIDA chamber, Atmos. Meas. Tech., 5, 3077–3097, https://doi.org/10.5194/amt-5-3077-2012, 2012c.

Lack, D. A., Langridge, J. M., Bahreini, R., Cappa, C. D., Middlebrook, A. M., and Schwarz, J. P.: Brown carbon and internal mixing in biomass burning particles, Proceedings of the National Academy of Sciences, 109, 14 802–14 807, https://doi.org/10.1073/pnas.1206575109, 2012.

Lamb, K. D.: Classification of iron oxide aerosols by a single particle soot photometer using supervised machine learning, Atmos. Meas. Tech. Discuss., pp. 1–30, https://doi.org/10.5194/amt-2019-106, 2019.

Laskin, A., Laskin, J., and Nizkorodov, S. A.: Chemistry of atmospheric brown carbon, Chem. Rev., 115, 4335–4382, https://doi.org/10.1021/cr5006167, 2015.

Liu, C., Chung, C. E., Zhang, F., and Yin, Y.: The colors of biomass burning aerosols in the atmosphere, Sci. Rep., 6, https://doi.org/10.1038/srep28267, 2016.

Liu, D., Whitehead, J., Alfarra, M. R., Reyes-Villegas, E., Spracklen, D. V., Reddington, C. L., Kong, S., Williams, P. I., Ting, Y.-C., Haslett, S., Taylor, J. W., Flynn, M. J., Morgan, W. T., McFiggans, G., Coe, H., and Allan, J. D.: Black-carbon absorption enhancement in the atmosphere determined by particle mixing state, Nat. Geosci., 10, 184–188, https://doi.org/10.1038/ngeo2901, 2017.

Liu, J., Scheuer, E., Dibb, J., Diskin, G. S., Ziemba, L. D., Thornhill, K. L., Anderson, B. E., Wisthaler, A., Mikoviny, T., Devi, J. J., Bergin, M., Perring, A. E., Markovic, M. Z., Schwarz, J. P., Campuzano-Jost, P., Day, D. A., Jimenez, J. L., and Weber, R. J.: Brown carbon aerosol in the North American continental troposphere: sources, abundance, and radiative forcing, Atmos. Chem. Phys., 15, 7841–7858, https://doi.org/10.5194/acp-15-7841-2015, 2015.

Liu, L. and Mishchenko, M. I.: Effects of aggregation on scattering and radiative properties of soot aerosols, J. Geophys. Res., 110, https://doi.org/10.1029/2004jd005649, 2005.

Michelsen, H., Schulz, C., Smallwood, G., and Will, S.: Laser-induced incandescence: Particulate diagnostics for combustion, atmospheric, and industrial applications, Prog. Energy Combust. Sci., 51, 2–48, https://doi.org/10.1016/j.pecs.2015.07.001, 2015.

Minutolo, P., Gambi, G., and D'Alessio, A.: The optical band gap model in the interpretation of the UV-visible absorption spectra of rich premixed flames, Symp. (Int.) Combust., 26, 951–957, https://doi.org/10.1016/s0082-0784(96)80307-9, 1996.

Moschos, V., Kumar, N. K., Daellenbach, K. R., Baltensperger, U., Prévôt, A. S. H., and Haddad, I. E.: Source Apportionment of Brown Carbon Absorption by Coupling Ultraviolet–Visible Spectroscopy with Aerosol Mass Spectrometry, Environmental Science & Technology Letters, 5, 302–308, https://doi.org/10.1021/acs.estlett.8b00118, 2018.

Moteki, N. and Kondo, Y.: Effects of Mixing State on Black Carbon Measurements by Laser-Induced Incandescence, Aerosol Sci. Technol., 41, 398–417, https://doi.org/10.1080/02786820701199728, 2007.

Moteki, N. and Kondo, Y.: Method to measure time-dependent scattering cross sections of particles evaporating in a laser beam, J. Aerosol Sci., 39, 348–364, https://doi.org/10.1016/j.jaerosci.2007.12.002, 2008.

Moteki, N. and Kondo, Y.: Dependence of Laser-Induced Incandescence on Physical Properties of Black Carbon Aerosols: Measurements and Theoretical Interpretation, Aerosol Sci. Technol., 44, 663–675, https://doi.org/10.1080/02786826.2010.484450, 2010.

Moteki, N., Kondo, Y., and Nakamura, S.: Method to measure refractive indices of small nonspherical particles: Application to black carbon particles, J. Aerosol Sci., 41, 513–521, https://doi.org/10.1016/j.jaerosci.2010.02.013, 2010.

Moteki, N., Kondo, Y., and Adachi, K.: Identification by single-particle soot photometer of black carbon particles attached to other particles: Laboratory experiments and ground observations in Tokyo, Journal of Geophysical Research: Atmospheres, 119, 1031–1043, https://doi.org/10.1002/2013jd020655, 2014.

Moteki, N., Adachi, K., Ohata, S., Yoshida, A., Harigaya, T., Koike, M., and Kondo, Y.: Anthropogenic iron oxide aerosols enhance atmospheric heating, Nat. Commun., 8, 15 329, https://doi.org/10.1038/ncomms15329, 2017.

Niemi, J. V., Saarikoski, S., Tervahattu, H., Mäkelä, T., Hillamo, R., Vehkamäki, H., Sogacheva, L., and Kulmala, M.: Changes in background aerosol composition in Finland during polluted and clean periods studied by TEM/EDX individual particle analysis, Atmos. Chem. Phys., 6, 5049–5066, https://doi.org/10.5194/acp-6-5049-2006, 2006.

550 Onasch, T., Trimborn, A., Fortner, E., Jayne, J., Kok, G., Williams, L., Davidovits, P., and Worsnop, D.: Soot Particle Aerosol Mass Spectrometer: Development, Validation and Initial Application, submitted, 2011.

Onasch, T. B., Trimborn, A., Fortner, E. C., Jayne, J. T., Kok, G. L., Williams, L. R., Davidovits, P., and Worsnop, D. R.: Soot Particle Aerosol Mass Spectrometer: Development, Validation, and Initial Application, Aerosol Sci. Technol., 46, 804–817, https://doi.org/10.1080/02786826.2012.663948, 2012.

555 Parent, P., Laffon, C., Marhaba, I., Ferry, D., Regier, T., Ortega, I., Chazallon, B., Carpentier, Y., and Focsa, C.: Nanoscale characterization of aircraft soot: A high-resolution transmission electron microscopy, Raman spectroscopy, X-ray photoelectron and near-edge X-ray absorption spectroscopy study, Carbon, 101, 86–100, https://doi.org/10.1016/j.carbon.2016.01.040, 2016.

Petzold, A., Ogren, J., Fiebig, M., Laj, P., Li, S.-M., Baltensperger, U., Holzer-Popp, T., Kinne, S., Pappalardo, G., Sugimoto, N., Wehrli, C., Wiedensohler, A., and Zhang, X.-Y.: Recommendations for the interpretation of "black carbon" measurements, Atmos. Chem. Phys., 13, 8365–8379, https://doi.org/10.5194/acp-13-8365-2013, 2013.

560 Pósfai, M., Gelencsér, A., Simonics, R., Arató, K., Li, J., Hobbs, P. V., and Buseck, P. R.: Atmospheric tar balls: Particles from biomass and biofuel burning, J. Geophys. Res. Atmos., 109, n/a–n/a, https://doi.org/10.1029/2003JD004169, 2004.

Saleh, R., Cheng, Z., and Atwi, K.: The Brown–Black Continuum of Light-Absorbing Combustion Aerosols, Environmental Science & Technology Letters, https://doi.org/10.1021/acs.estlett.8b00305, 2018.

565 Schwarz, J. P., Gao, R. S., Fahey, D. W., Thomson, D. S., Watts, L. A., Wilson, J. C., Reeves, J. M., Darbeheshti, M., Baumgardner, D. G., Kok, G. L., Chung, S. H., Schulz, M., Hendricks, J., Lauer, A., Kärcher, B., Slowik, J. G., Rosenlof, K. H., Thompson, T. L., Langford, A. O., Loewenstein, M., and Aikin, K. C.: Single-particle measurements of midlatitude black carbon and light-scattering aerosols from the boundary layer to the lower stratosphere, J. Geophys. Res., 111, D16 207, https://doi.org/10.1029/2006JD007076, 2006.

Sedlacek, A. J., Lewis, E. R., Kleinman, L., Xu, J., and Zhang, Q.: Determination of and evidence for non-core-shell structure of particles
570 containing black carbon using the Single-Particle Soot Photometer (SP2), Geophys. Res. Lett., 39, https://doi.org/10.1029/2012gl050905, 2012.

Sedlacek, A. J., Lewis, E. R., Onasch, T. B., Lambe, A. T., and Davidovits, P.: Investigation of Refractory Black Carbon-Containing Particle Morphologies Using the Single-Particle Soot Photometer (SP2), Aerosol Sci. Technol., 49, 872–885, https://doi.org/10.1080/02786826.2015.1074978, 2015.

575 Sedlacek, A. J., Onasch, T. B., Nichman, L., Lewis, E. R., Davidovits, P., Freedman, A., and Williams, L.: Formation of refractory black carbon by SP2-induced charring of organic aerosol, Aerosol Sci. Technol., 52, 1345–1350, https://doi.org/10.1080/02786826.2018.1531107, 2018.

Sedlacek III, A. J., Buseck, P. R., Adachi, K., Onasch, T. B., Springston, S. R., and Kleinman, L.: Formation and evolution of Tar Balls from Northwestern US wildfires, Atmos. Chem. Phys. Discuss., pp. 1–28, https://doi.org/10.5194/acp-2018-41, 2018.

Semeniuk, T. A., Wise, M. E., Martin, S. T., Russell, L. M., and Buseck, P. R.: Hygroscopic behavior of aerosol particles from biomass fires
580 using environmental transmission electron microscopy, J. Atmos. Chem., 56, 259–273, https://doi.org/10.1007/s10874-006-9055-5, 2006.

Slowik, J. G., Cross, E. S., Han, J.-H., Davidovits, P., Onasch, T. B., Jayne, J. T., Williams, L. R., Canagaratna, M. R., Worsnop, D. R., Chakrabarty, T. K., Moosmüller, J., Arnott, E. P., Schwarz, J. P., Gao, R.-S., Fahey, F. W., Kok, G. L., and Petzold, A.: An Inter-Comparison of Instruments Measuring Black Carbon Content of Soot Particles, Aerosol Sci. Technol., 41, 295–314, https://doi.org/10.1080/02786820701197078, 2007.

585 Stephens, M., Turner, N., and Sandberg, J.: Particle identification by laser-induced incandescence in a solid-state laser cavity, Appl. Opt., 42, 3726–3736, https://doi.org/10.1364/AO.42.003726, 2003.

Taylor, J., Allan, J., Liu, D., Flynn, M., Weber, R., Zhang, X., Lefer, B., Grossberg, N., Flynn, J., and Coe, H.: Assessment of the sensitivity of core/shell parameters derived using the single-particle soot photometer to density and refractive index, Atmos. Meas. Tech., 8, 1701–1718, https://doi.org/10.5194/amt-8-1701-2015, 2015.

590 Tivanski, A. V., Hopkins, R. J., Tyliszczak, T., and Gilles, M. K.: Oxygenated Interface on Biomass Burn Tar Balls Determined by Single Particle Scanning Transmission X-ray Microscopy, J. Phys. Chem. A, 111, 5448–5458, https://doi.org/10.1021/jp070155u, 2007.

Tóth, A., Hoffer, A., Nyirő-Kósa, I., Pósfai, M., and Gelencsér, A.: Atmospheric tar balls: aged primary droplets from biomass burning?, Atmos. Chem. Phys., 14, 6669–6675, https://doi.org/10.5194/acp-14-6669-2014, 2014.

Tóth, Á., Hoffer, A., Pósfai, M., Ajtai, T., Kónya, Z., Blazsó, M., Czégény, Z., Kiss, G., Bozóki, Z., and Gelencsér, A.: Chemical characterization
595 of laboratory-generated tar ball particles, Atmos. Chem. Phys., 18, 10 407–10 418, https://doi.org/10.5194/acp-18-10407-2018, 2018.

Vander Wal, R. L., Bryg, V. M., and Huang, C.-H.: Aircraft engine particulate matter: Macro- micro- and nanostructure by HRTEM and chemistry by XPS, Combust. Flame, 161, 602–611, https://doi.org/10.1016/j.combustflame.2013.09.003, 2014.

Vernooij, M. G. C., Mohr, M., Tzvetkov, G., Zelenay, V., Huthwelker, T., Kaegi, R., Gehrig, R., and Grobéty, B.: On Source Identification and Alteration of Single Diesel and Wood Smoke Soot Particles in the Atmosphere; An X-Ray Microspectroscopy Study, Environ. Sci.
600 Technol., 43, 5339–5344, https://doi.org/10.1021/es800773h, 2009.

Zangmeister, C. D., You, R., Lunny, E. M., Jacobson, A. E., Okumura, M., Zachariah, M. R., and Radney, J. G.: Measured in-situ mass absorption spectra for nine forms of highly-absorbing carbonaceous aerosol, Carbon, 136, 85–93, https://doi.org/10.1016/j.carbon.2018.04.057, 2018.

Zhu, J., Crozier, P. A., and Anderson, J. R.: Characterization of light-absorbing carbon particles at three altitudes in East Asian outflow by
605 transmission electron microscopy, Atmos. Chem. Phys., 13, 6359–6371, https://doi.org/10.5194/acp-13-6359-2013, 2013.